ELSEVIER

Journal of Power Sources 68 (1997) 570–577

JOURNAL OF POWER SOURCES

Structural and electrochemical studies of α-manganese dioxide (α-MnO_2) [1]

C.S. Johnson [a,*], D.W. Dees [a], M.F. Mansuetto [a], M.M. Thackeray [a], D.R. Vissers [a], D. Argyriou [d], C.-K. Loong [c], L. Christensen [b]

[a] *Electrochemical Technology Program, Chemical Technology Division, Argonne National Laboratory, Argonne, IL 60439, USA*
[b] *Electrochemical Technology Program, Materials Science Division, Argonne National Laboratory, Argonne, IL 60439, USA*
[c] *Electrochemical Technology Program, Intense Pulsed Neutron Source Division, Argonne National Laboratory, Argonne, IL 60439, USA*
[d] *3M Corporation, 3M Center, St. Paul, MN 55144, USA*

Accepted 28 October 1996

Abstract

The structural and electrochemical properties of α-MnO_2, prepared by acid digestion of Mn_2O_3, and its lithiated derivatives $xLi_2O \cdot MnO_2$ ($0 \le x \le 0.25$) have been investigated as insertion compounds in the search for new and viable cathode materials for rechargeable 3 V batteries. The α-MnO_2 product fabricated by this technique contains water within the large (2×2) channels of the structure; the water can be removed from the α-MnO_2 framework without degradation of the structure, and then at least partially replaced by Li_2O (lithium oxide). The Li_2O-doped α-MnO_2 electrodes, described generically as xLi_2O MnO_2, stabilize the structure and provide higher capacities on cycling than the parent material. The structures of these α-MnO_2-type electrode materials are described, and electrochemical data are presented for both liquid electrolyte and polymer electrolyte Li/α-MnO_2 and Li/$xLi_2O \cdot MnO_2$ cells. © 1997 Published by Elsevier Science S.A.

Keywords: Manganese dioxide, Lithium batteries, Structure; Electrochemical properties

1. Introduction

Manganese oxides are of interest as insertion electrodes for primary and secondary lithium batteries [1]: (i) heat-treated α-MnO_2 electrodes are used in commercial 3 V primary cells; (ii) electrodes consisting of an intergrowth structure of lithiated α-MnO_2 and spinel-related MnO_2 are used in commercial 3 V rechargeable cells, and (iii) the spinel system $Li_x[Mn_2]O_4$ ($0 < x \le 1$) is being developed for 4 V rechargeable lithium cells. The rechargeability of 3 V manganese oxide electrodes tends to be limited by the anisotropic expansion and contraction of the crystallographic unit cell when lithium is inserted into, and removed from, α-MnO_2 or spinel-related electrode structures. Crystallographic distortions in lithiated manganese oxides can be attributed largely to a Jahn–Teller effect, where the concentration of Mn^{3+} ions within the oxygen array reaches a critical value, typically when the mean oxidation state of manganese falls below 3.5 [2]. For example, in the 3 V spinel electrode system $Li_x[Mn_2]O_4$ ($1 < x \le 2$), the onset of the Jahn–Teller effect at $x = 1$ results in a tetragonal distortion of the unit cell [3]; the 16% increase in the c/a ratio is too severe for the crystal structure to tolerate repeated charge and discharge cycles. The practical consequence of this distortion is, therefore, a pronounced loss in capacity in the spinel cathode during cycling of the cell. Alternative lithium manganese oxide 3 V electrodes exist and offer advantages over the 3 V $Li_x[Mn_2]O_4$ spinel electrode. A notable example is the intergrowth structure of lithiated α-MnO_2 and spinel-related MnO_2 which yields superior electrochemical cycling. However, the performance of 3 V MnO_2 electrodes still needs to be improved in terms of both electrode capacity and stability.

A potentially attractive alternative material for 3 V rechargeable lithium battery systems is α-manganese dioxide (α-MnO_2) [4]. A reversible capacity exceeding 160 mAh/g has been reported for a lithiated α-MnO_2 electrode that was synthesized by ion exchange of Li^+ for NH_4^+ in $NH_4Mn_8O_{16}$ [5]. It was recently reported that a highly pure and crystalline α-MnO_2 product can be synthesized by a simple route involving acid digestion of Mn_2O_3 [6,7]. X-ray and neutron dif-

* Corresponding author.

[1] This paper has been authored by a contractor of the US Government under Contract No. W-31-109-ENG-38. Accordingly, the US Government retains a nonexclusive, royalty-free license to publish or reproduce the published form of this contribution, or allow others to do so, for US Government purposes.

0378-7753/97/$17.00
PII S0378-7753(96)02633-X

fraction studies have suggested that this α-MnO_2 product is devoid of any 'stabilizing' cation or molecule, other than H_3O^+ or H_2O, within the (2×2) tunnel [8]. Electrochemical cycling studies of these materials, however, were disappointing, resulting in capacities of about 120 mAh/g after 20 cycles.

In this work, we have synthesized α-MnO_2 materials from two Mn_2O_3 precursors. We have also fabricated Li_2O-doped α-MnO_2 products in an attempt to stabilize the electrode structure and to improve its electrochemical properties. Materials were analyzed in terms of their structural and electrochemical properties in order to obtain a better understanding of the factors that control and affect the rechargeability of α-MnO_2 insertion electrodes in lithium cells.

2. Experimental

The synthesis of hydrated α-manganese dioxide (α-$MnO_2 \cdot nH_2O$; $n \approx 0.2$–0.36) was carried out in two steps. In the first step, Mn_2O_3 was prepared by heating either electrolytic α-MnO_2 powder (EMD, Kerr–McGee Corporation) or chemically-prepared α-MnO_2 (CMD, Chemetals Inc.) in air at 700 °C. In the second step, Mn_2O_3 was reacted with 4–8 M H_2SO_4 at 105 °C, which resulted in the disproportionation of Mn_2O_3 into a soluble Mn^{2+} species and the desired α-MnO_2 product. The reaction temperature can be decreased to 40 °C if the time for reaction is increased to days instead of hours. The resulting product was dehydrated at 300 °C. The α-MnO_2 powders were lithiated with n-butyllithium (25% mole excess) at −40 °C or with LiI (50% mole excess) at −40, 25, and 80 °C. Li_2O-doped products ($xLi_2O \cdot MnO_2$; $0 \le x \le 0.25$) were prepared by reaction of α-MnO_2 with $LiOH \cdot H_2O$ by wet mixing in methanol, drying the resulting slurry, and firing the final mixture in air at 275 °C.

The water content in α-MnO_2 samples was measured by thermogravimetric methods. Manganese and lithium contents were determined by using inductively-coupled atomic emission spectroscopy with an Instruments SA JY86 spectrometer. Hydrogen analysis was carried out on a LECO-900 analyzer. The oxygen content in α-MnO_2 samples was determined by a potentiometric titration method [9]. Samples were checked for elemental purity by X-ray fluorescence (XRF) and energy-dispersive analysis of X-rays (EDAX) at Michigan Technological University; these analyses revealed only trace quantities of residual sulfur, potassium, and barium.

Inelastic neutron scattering and neutron diffraction experiments were conducted on the High-Resolution Medium-Energy Chopper spectrometer (HRMECS) and Special Environment Powder Diffractometer (SEPD), respectively, at the Intense Pulsed Neutron Source (IPNS) at Argonne National Laboratory. X-ray diffraction patterns were collected on an automated Siemens D5000 powder diffractometer with Cu Kα radiation. Unit-cell parameters were calculated by a least-squares refinement of the X-ray diffraction peak positions. The structures of hydrated, heat-treated, and Li_2O-doped α-MnO_2 samples were refined from powder neutron-diffraction patterns with the Rietveld profile refinement program GSAS [10]. Initial parameters for the refinement were taken from a previously reported structure of α-MnO_2 derived from Li_2MnO_3 [11].

Electrochemical testing of Li/α-MnO_2 cells was conducted with a fully automated Maccor battery control unit, using either a button cell (size 2016, or 1225) with a liquid electrolyte or a thin (< 100 μm) polymer electrolyte cell. The liquid electrolyte was 1 M $LiPF_6$ in 1:1 EC:DMC (FMC, Lithium Division); the solid polymer electrolyte (SPE), which was supplied by 3M Corporation, consisted of a poly(ethylene oxide)-based system containing a solvated lithium bis-trifluoromethanesulfonyl imide salt [$LiN(CF_3SO_2)_2$]. Cathode pellets (in two sizes, surface area ≈ 1 or 0.5 cm^2) for the button cells consisted typically of 80 wt.% oxide, 8 wt.% poly(vinylidene fluoride) (PVDF) binder (Aldrich), 10 wt.% carbon (Cabot, Vulcan XC-72), and 2 wt.% natural graphite (Aldrich). The cathode laminates for the polymer cells (surface area: 3.89 cm^2) were supplied by 3M Corporation and consisted typically of 62.5 wt.% oxide, 3 wt.% carbon (Ketjen black), and 34.5 wt.% polymer salt complex. Metallic lithium foil anodes (FMC, Lithium Division) were used for both the button cells and the polymer electrolyte cells. Cells were assembled in a helium-filled (O_2 < 2.0 ppm) recirculating and purification glove box.

Two electrodes were used for cyclic voltammetry studies of the polymer electrolyte cells. In these experiments, lithium foil was used for the reference and counter electrodes. To minimize electrode polarization effects, the surface area of the combined lithium foil counter/reference electrode was much larger than the surface area of the cathode pellet (~ 1 mm^2).

3. Results and discussion

3.1. Structure analyses of hydrated and dehydrated α-MnO_2

The X-ray diffraction patterns of various α-MnO_2 products that originated from an Mn_2O_3 precursor are shown in Fig. 1(a)–(e). The average lattice parameters of the tetragonal unit cell ($I4/m$) were determined from 10 separate hydrated α-$MnO_2 \cdot nH_2O$ samples (Fig. 1(a)) to be $a = b = 9.813$ Å and $c = 2.850$ Å. Hydrated α-$MnO_2 \cdot nH_2O$ samples, analyzed by thermogravimetry, were found to contain about 4–7 wt.% water ($n \approx 0.20$–0.36). A hydrogen analysis of one α-$MnO_2 \cdot nH_2O$ sample yielded a hydrogen content of 0.73 wt.%, in good agreement with the value expected from the water content measured by thermal analysis. The unit cell contracts by approximately 0.9% upon heat treatment at 275 °C, with a and b contracting by 0.6% and c increasing by 0.4% (see Table 1 and Fig. 1(b)). This finding

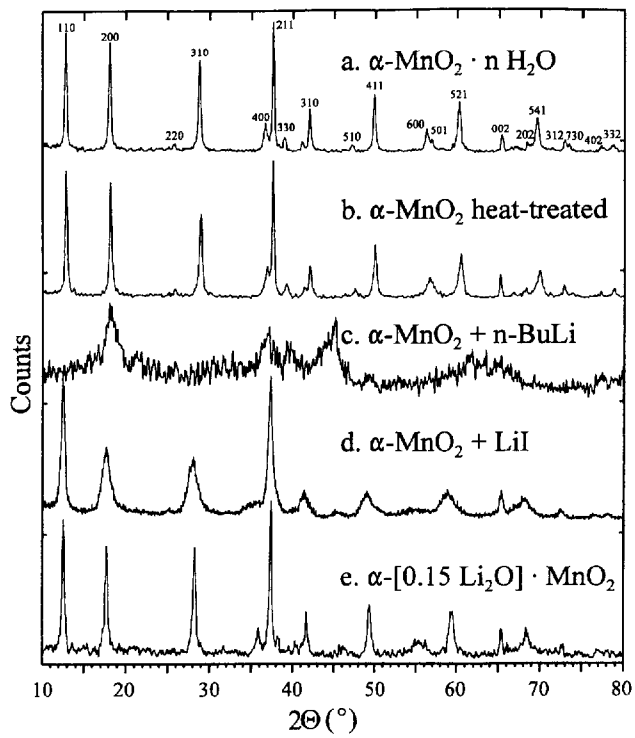

Fig. 1. X-ray powder diffraction patterns of α-MnO_2 samples (a) α-$MnO_2 \cdot nH_2O$; (b) heat-treated α-MnO_2 (275 °C); (c) Li_xMnO_2 from n-butyllithium reaction (−40 °C); (d) Li_xMnO_2 from LiI reaction (25 °C), and (e) $0.15Li_2O \cdot MnO_2$.

Table 1
Lattice parameters of α-$[xLi_2O] \cdot MnO_2$ (space group $I4/m$)

Compound	a (Å)	c (Å)
α-MnO_2 (hydrated)	9.8107(8)	2.8502(5)
α-MnO_2 (dehydrated)	9.7502(9)	2.8607(6)
$0.05Li_2O \cdot MnO_2$	9.8180(10)	2.8595(7)
$0.10Li_2O \cdot MnO_2$	9.9035(9)	2.8531(7)
$0.15Li_2O \cdot MnO_2$	9.9646(8)	2.8499(7)
$0.20Li_2O \cdot MnO_2$	9.9567(8)	2.8499(6)
$0.25Li_2O \cdot MnO_2$	9.9568(11)	2.8475(8)

is evidence that the hydrated sample contains lattice-specific structural water.

The structures of hydrated and dehydrated α-MnO_2 samples were refined with time-of-flight neutron-diffraction data; the gross structural features are effectively identical to those of α-MnO_2 products synthesized by acid digestion of Li_2MnO_3 [8]. Water molecules reside in the (2×2) channels of the structure, with the oxygen ions from the water being located at (0.0, 0.0, 0.50), which is close to the position normally occupied by 'stabilizing' cations, such as K^+ in cryptomelane (KMn_8O_{16}) [12]. The refinement of the dehydrated product confirmed earlier reports that the water can be entirely removed from α-MnO_2, and that this framework structure is stable to at least 300 °C [7]. The structure of the anhydrous α-MnO_2 product is shown in Fig. 2.

Interactions between the H_2O molecules within the structure were assessed by inelastic neutron scattering measurements. The inelastic neutron cross-section scattering coefficient of hydrogen is at least one order of magnitude greater than that of manganese or oxygen. Thus, the intensities of bands in the energy-transfer spectra are predominantly due to hydrogen interactions within the structure. Fig. 3(a) shows a representative, baseline-corrected spectrum of α-$MnO_2 \cdot 0.25H_2O$ obtained with a neutron incident energy of 600 meV. An assignment of the vibrational modes due to the

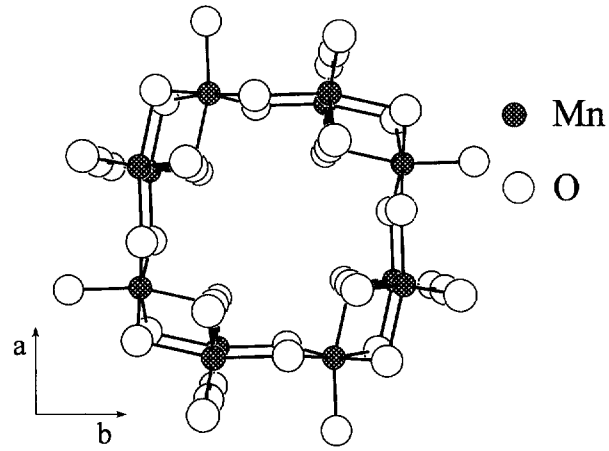

Fig. 2. The structure of heat-treated α-MnO_2 as viewed down the c-axis showing the empty (2×2) channel.

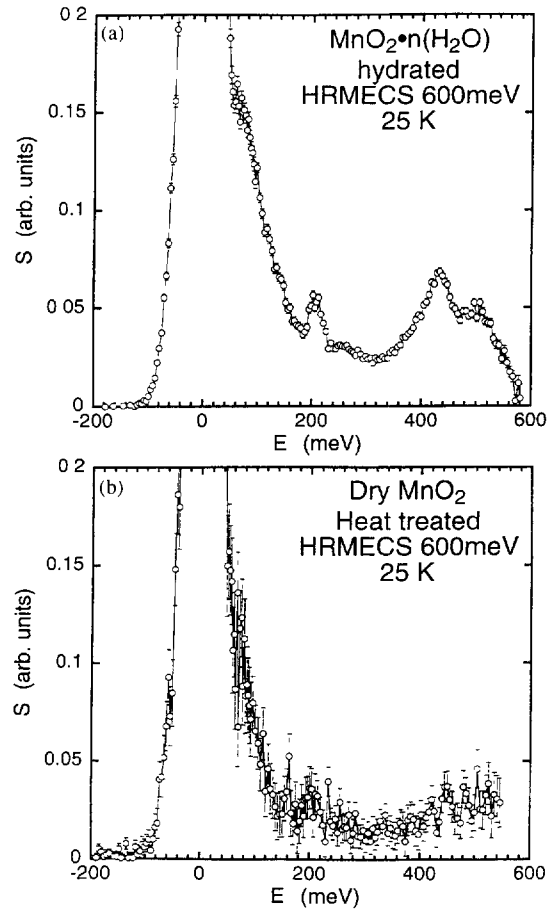

Fig. 3. Inelastic neutron scattering spectra for (a) α-MnO_2 $0.25H_2O$, and (b) heat treated α-MnO_2 (275 °C) made from a.

Table 2
Inelastic neutron scattering results on hydrated α-MnO_2

Peak Number	Energy		Relative intensity	Assignment
	meV	cm^{-1}		
1	4	32	weak, narrow	H_4^+ rotation [a]
2	13	105	weak, narrow	H_2O translation
3	12–18	97–145	medium, broad	lattice vibration
4	22–27	177–217	medium, broad	lattice vibration
5	36	290	weak, narrow	lattice vibration
6	65	524	strong, broad	$\tau(H_2O)$ rotation
7	90	725	medium, broad	Mn–O stretch
8	110	887	weak, broad	Mn–O stretch
9	140	1129	medium, narrow	HOH bend (op)
10	200	1613	strong, narrow	HOH bend (ip)
11	420	3387	strong, broad	–OH group stretch
12	490	3952	medium, broad	combination mode

[a] H_4^+ tetrahedra have been suggested by others to replace Mn^{4+} vacancies in MnO_2 materials [14].

water and the MnO_2 lattice is summarized in Table 2 [13,14]. Four incident energies (50, 150, 250, and 600 meV) were used for complete analysis. Fig. 3(b) represents the spectrum of the same sample after heat treatment at 275 °C. This spectrum is essentially featureless in terms of hydrogen interactions and confirms that water is removed from α-MnO_2 on heat treatment. (Note that the presence of a large continuum background in the spectrum of the hydrated sample suggests significant mobility of hydrogen ions.) Further work is in progress to model and quantify the diffusivity of H^+ in α-MnO_2 materials.

3.2. Chemical lithiation of α-MnO_2

Reaction of dehydrated α-MnO_2 with an excess of a strong reducing agent, such as *n*-butyllithium to produce Li_xMnO_2 ($x \approx 1$), destroys the α-MnO_2 framework structure, as is evident from X-ray diffraction patterns of lithiated products, which show broad peaks in positions characteristic of a spinel-type structure (Fig. 1(c)). Use of a milder lithiating agent, such as LiI, retains the α-MnO_2 framework, although a broadening of the X-ray diffraction peaks occurs (Fig. 1(d)). In this reaction, the degree of lithiation is limited ($x < 0.5$) because of the lower reduction potential of LiI (approximately 3.0 V versus Li) [15]. For example, the reaction

$$MnO_2 + 1.5LiI \rightarrow Li_xMnO_2 + 0.5 - x/3LiI_3 \quad (1)$$

results in $x = 0.1$ at -40 °C and $x = 0.42$ at 25 °C. Lithiation at 80 °C results in a breakdown of the α-MnO_2 structure. The instability of pure α-MnO_2 to high levels of lithiation is believed to be a major reason for the poor rechargeability of Li/α-MnO_2 cells.

3.3. Reaction of α-MnO_2 with LiOH

Ion-exchange reactions of 'cation-stabilized' α-MnO_2 materials, such as $NH_4Mn_8O_{16}$, with LiOH at moderate temperature (300 °C) has demonstrated that lithiated α-MnO_2 products provide superior electrochemical properties to those of the parent α-MnO_2 compound [4]. For example, lithiated products derived from $NH_4Mn_8O_{16}$ deliver capacities of 160 mAh/g, in contrast to the 100 mAh/g of the parent material [5]. The parent compound and lithiated product made by this route, referred to generically as $xLi_2O \cdot MnO_2$, tend to be poorly crystalline materials, making structure analysis of the initial electrode and discharged products difficult [16,17]. The successful synthesis of highly crystalline, anhydrous α-MnO_2 products from Mn_2O_3, therefore, raises the possibility of determining structural features of $xLi_2O \cdot MnO_2$ electrode materials that would explain the enhanced electrochemical behavior of these lithiated α-MnO_2 electrodes over the parent α-MnO_2 compound.

In this study, α-MnO_2 products were reacted with LiOH in various ratios. Table 1 lists the lattice parameter data of various $xLi_2O \cdot MnO_2$ products for $0 \leq x \leq 0.25$. Redox titrations on samples of heat-treated α-MnO_2 and $xLi_2O \cdot MnO_2$, first using ammonium ferrous sulfate to reduce the manganese ions to Mn^{2+} and then back-titrating the excess Fe^{2+} with a standard $KMnO_4$ solution, confirmed that the oxidation state of manganese was 4. The X-ray diffraction patterns of products to $x = 0.15$ were representative of a single-phase product, which is consistent with the progressive expansion of the *a*-lattice parameter with increasing the Li_2O content (Table 1). Products with $x > 0.2$ tended to be two-phase, with the X-ray patterns showing the onset of lithium manganese oxide spinel formation. Fig. 1(e) shows the X-ray diffraction pattern of $[0.15Li_2O] \cdot MnO_2$; the pattern shows that the Li_2O-doped product retains the gross structural features of the parent compound and also maintains a high degree of crystallinity.

3.4. Structure analysis of $0.15Li_2O \cdot MnO_2$

A neutron diffraction study was conducted on a lithiated α-MnO_2 sample of composition $0.15Li_2O \cdot MnO_2$. The structure, as determined from a Rietveld profile refinement is depicted in Fig. 4. A difference Fourier map provided evidence that the oxygen ion from the Li_2O molecule was located at (0.0, 0.0, 0.40), with a site occupancy equal to 0.20(1). This is close to the position that was occupied by the oxygen ion of the H_2O molecule in the hydrated compound. A subsequent difference Fourier map (after subtraction of all the manganese and oxygen from the structure) indicated that the lithium ions were located at (0.204, 0.078, 0.000), with a site occupancy of 0.19(2). Within experimental error, the final structure analysis yielded a composition of $0.10Li_2O \cdot MnO_2$, which is considered to be in very good agreement with the anticipated composition of $0.15Li_2O \cdot MnO_2$, given the low concentration of Li_2O in the compound and the quality of the data. Interatomic Li–O distances showed that the lith-

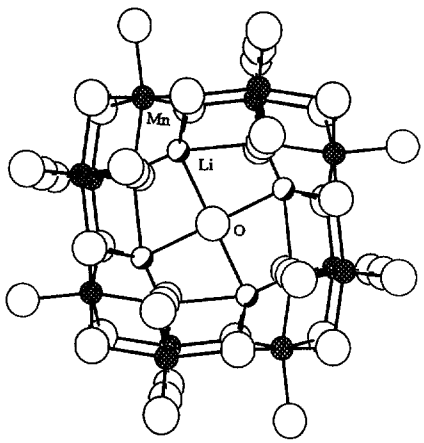

Fig 4. The structure of $0.15Li_2O \cdot MnO_2$ viewed down the c-axis, showing the position and coordination of additional lithium with oxygen.

ium ions were coordinated more strongly with the oxygens of the framework structure than with the oxygens in the (2×2) tunnels. (Note that if an oxygen ion completely occupied the site at (0.0, 0.0, 0.5), then a distorted hexagonal, close-packed oxygen array would result, similar to that found in α-MnO_2 structures.) These data, therefore, indicate that the role of Li_2O is to stabilize α-MnO_2 structures, with oxygen occupying sites in the defect oxygen array of the α-MnO_2 framework, and with the charge-compensating lithium ions occupying newly created interstitial sites. A more detailed description of Li_2O-stabilized α-MnO_2 structures has been presented elsewhere [18].

3.5. Chemical lithiation of $0.15Li_2O \cdot MnO_2$

To compare the tolerance of $xLi_2O \cdot MnO_2$ products with chemical lithiation with pure α-MnO_2, the $0.15Li_2O \cdot MnO_2$ ($x = 0.15$) powder was reacted with LiI at 0, 25, and 80 °C, according to the reaction

$$[0.15Li_2O] \cdot MnO_2 + 1.5LiI \rightarrow Li_x[0.15Li_2O] \cdot MnO_2 + 0.5 - x/3LiI_3 \quad (2)$$

The reaction at 80 °C resulted in structural degradation, as with α-MnO_2. At 25 °C, x was analyzed to be 0.26. The X-ray diffraction pattern of the $Li_{0.26}[0.15Li_2O] \cdot MnO_2$ product prepared at 25 °C was indicative of a considerably more crystalline material than a corresponding Li_xMnO_2 product prepared at the same temperature, thereby providing additional evidence that $xLi_2O \cdot MnO_2$ electrodes should provide better tolerance to lithiation than does pure α-MnO_2 itself. The lattice parameters of the various starting materials and products lithiated with LiI at 25 °C are listed in Table 3.

Table 3 shows that the volume of the unit cell of α-MnO_2 increased by 5.07% when 0.42Li were inserted into the α-MnO_2 framework, whereas $0.15Li_2O \cdot Li_xMnO_2$, which could only take up 0.26Li at the same temperature, increased by 4.25%. Note that the volume expansion occurs predominantly because of the increase in a and b, and that the c-parameter, which reflects an O–O distance, remains effectively constant.

Table 3
Unit cell parameters from XRD for α-MnO_2 and chemically lithiated products (space group: $I4/m$)

Compound	a (Å)	c (Å)	Volume (Å^3)	% Change
α-MnO_2 (dehydrated)	9.766	2.861	272.9	
$Li_{0.42}MnO_2$	10.039	2.852	287.4	5.07
$[0.15Li_2O] \cdot MnO_2$	9.942	2.851	281.8	
$Li_{0.26}[0.15Li_2O] \cdot MnO_2$	10.169	2.846	294.3	4.25

In principle, therefore, the Jahn–Teller distortion, which is expected to occur when the average Mn oxidation state reaches 3.5, can be accommodated in tetragonal α-MnO_2 materials in two dimensions, rather than in one dimension (as is the case in the spinel system $Li_x[Mn_2]O_4$, which undergoes a cubic-tetragonal distortion when x exceeds 1 [2]). This observation has implications for designing improved manganese oxide materials that will be more tolerant to lithium insertion/extraction reactions, particularly for rechargeable 3 V lithium cells.

4. Electrochemical results

4.1. Liquid electrolyte cells

The Li/α-MnO_2 button cells (size 1225) were galvanostatically cycled at 0.1 mA between 3.5 and 2.0 V. The coulombic efficiency for the first charge was low (75%), but on the second charge cycle the cell showed good rechargeability, with a coulombic efficiency close to 100%. This observation suggests that some lithium ions that are inserted on the initial discharge become locked within the structure for stabilization purposes, and that voltages in excess of 3.5 V are necessary to electrochemically extract all the lithium from the electrode structure. In this test, the initial discharge capacity delivered by the Li/α-MnO_2 cell was 171 mAh/g and the capacity on

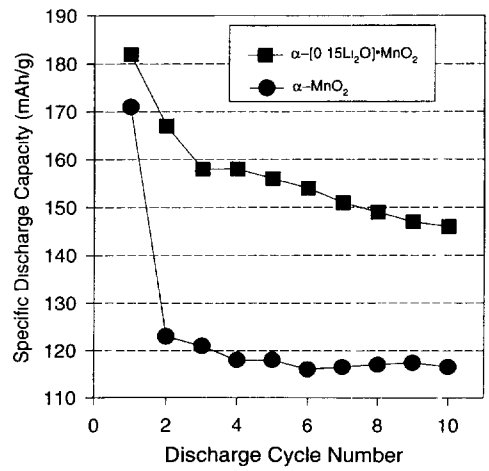

Fig. 5. Evolution of discharge capacity over the first ten cycles for liquid electrolyte button cells; voltage, 3.5–2.0 V, and current rate 0.1 mA

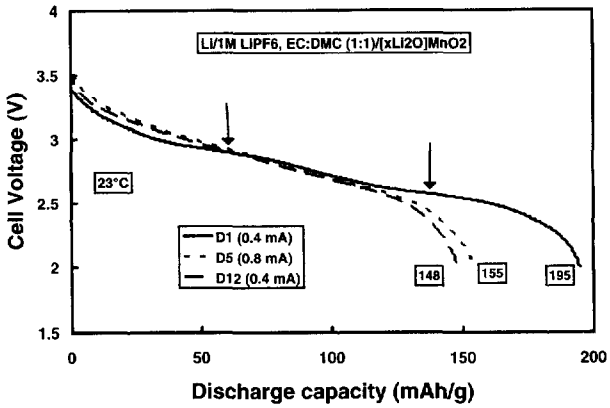

Fig. 6. Galvanostatic discharge curves for 0 $15Li_2O \cdot MnO_2$ electrodes in liquid electrolyte button cells (size 2016) The arrows indicate the plateaus on the first discharge.

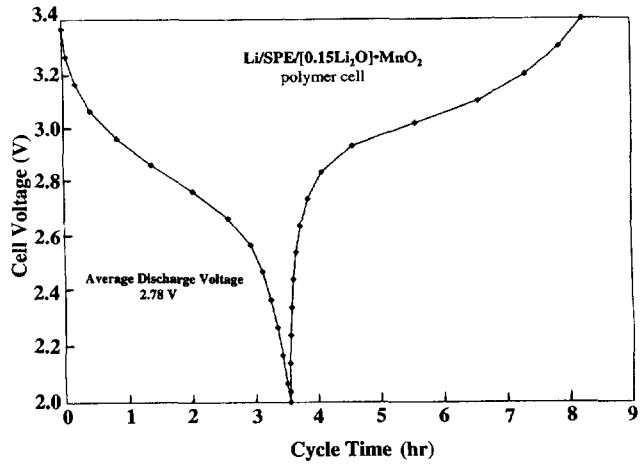

Fig. 8. The 84th discharge-charge cycle of a Li/1M $LiPF_6$, EC:DMC (1:1)/ $0.15Li_2O \cdot MnO_2$ button cell.

the second cycle was 123 mAh/g; thereafter, the cell stabilized, yielding a constant 117 mAh/g for 10 cycles (Fig. 5). By contrast, $Li/0.15Li_2O \cdot MnO_2$ cells showed excellent coulombic efficiency from the first cycle (98.9%), when discharged and charged over the same voltage range and at the same rate (0.1 mA). These cells delivered an initial discharge capacity of 182 mAh/g, which decreased to 158 mAh/g after three cycles, and thereafter lost capacity slowly over the next seven cycles to yield a capacity of 146 mAh/g after ten cycles (Fig. 5). This performance reflects a significant improvement over unstabilized α-MnO_2 electrodes.

Larger button cells (size 2016) of $Li/0.15Li_2O \cdot MnO_2$ were also built and charged and discharged successfully for more than 80 cycles without changing the lithium electrode. They showed good rate capability and could withstand a fourfold increase in current density (1.6 mA); increasing the rate to 1.6 mA at the tenth cycle resulted in only a 17% drop in capacity. After 80 cycles, the capacity delivered by the stabilized α-MnO_2 electrode, at 0.4 mA, was 130 mAh/g.

Fig. 6 shows that the first discharge profile (D1) of the $Li/0.15Li_2O \cdot MnO_2$ cell is characterized by two independent (slightly sloping) voltage plateaus (see arrows). With cycling, however, the plateaus disappear and the discharge adopts a single sloping profile, typical of a single-phase insertion electrode. With Li_2O-stabilized α-MnO_2 electrodes, the slope of the curve remains unchanged with increasing current (see discharge 5, D5, and discharge 12, D12, in Fig. 6). This finding implies good electrode kinetics and lithium cation diffusion. The profile of the 84th discharge/charge cycle is shown in Fig. 7. Current interrupts conducted at the end of discharge and charge indicated that the cell impedance did not change over the cycle life test.

4.2. Lithium polymer electrolyte cells

Preliminary studies have demonstrated that the electrochemical behavior of lithium-stabilized α-MnO_2 electrodes in room-temperature liquid electrolyte cells is similar to their behavior in lithium/polymer electrolyte cells operated at 60 °C (Fig. 8).

Fig. 9 shows a cyclic voltammogram of a composite electrode of $0.15Li_2O \cdot MnO_2$, using lithium foil as both the counter and the reference electrodes. The sweep rate was 0.06 mV/s, and the temperature of the cell was 100 °C. The two peaks observed in the voltammogram ($E^1_{pc} = 2.75$ V and $E^2_{pc} = 2.94$ V) on the twelfth sweep, at 100 °C, coalesce into a single reduction peak on cycling ($E_{pc} = 2.88$ V, cycle no.

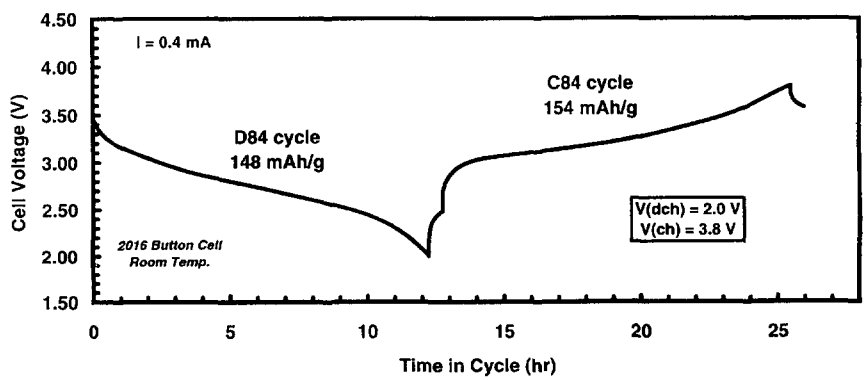

Fig. 7. Discharge/charge cycle no. 6 of a $Li/SPE/0.15Li_2O \cdot MnO_2$ cell at 0.6 mA rate recorded at 60 °C

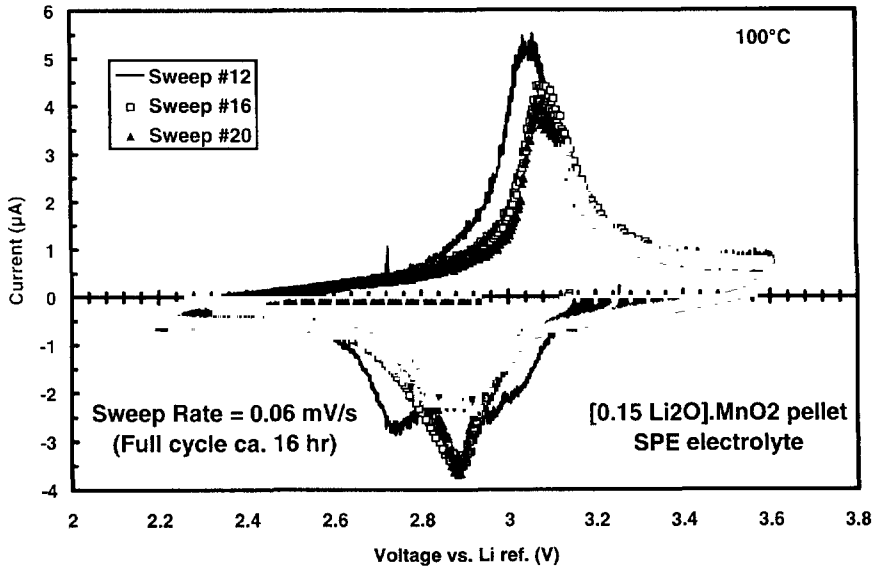

Fig. 9. Cyclic voltammograms of a $0.15Li_2O \cdot MnO_2$ electrode in a lithium/polymer electrolyte cell.

20). This phenomenon is consistent with the two plateaus seen on the first discharge cycle of button cells containing lithium-doped α-MnO_2 cathodes (see, for example, Fig. 6). Integration of the area under the reductive and oxidative peaks indicated that equal charge was transferred during discharge and charge, thus demonstrating excellent redox reversibility in the cathode.

The electrochemical and structural evaluation of these classes of MnO_2 materials in liquid and polymer electrolyte lithium cells are being continued.

5. Conclusions

Alpha-MnO_2, derived from Mn_2O_3, and Li_2O-stabilized MnO_2 products $xLi_2O \cdot MnO_2$ $(0 \leq x \leq 0.25)$ have been investigated in terms of their structural properties and electrochemical performance in lithium cells with either liquid electrolyte or polymer electrolyte. The data provide evidence that the α-MnO_2 structure is stabilized by oxygen ions from either H_2O or Li_2O molecules located within the (2×2) channels; the oxygen ions are accommodated at sites normally occupied by cations, such as Ba^{2+} in hollandite ($BaMn_8O_{16}$) and K^+ in cryptomelane (KMn_8O_{16}). Although not yet optimized, Li_2O-stabilized products, $xLi_2O \cdot MnO_2$ ($x \approx 0.15$), provide significantly superior capacity on cycling to the parent α-MnO_2 material. Products with $x > 0.2$ tend to have two-phases, consisting of a Li_2O-stabilized α-MnO_2 compound and a lithium–manganese-oxide spinel. Further work is required to enhance the cycling stability of α-MnO_2 materials derived from Mn_2O_3 before they can be considered commercially attractive for use in rechargeable 3 V lithium batteries.

Acknowledgements

The authors would like to thank the US Advanced Battery Consortium, 3M, and Hydro-Québec for supporting this work under CRADA Contract No. 9 203 901. Support for Argonne National Laboratory from the US Department of Energy under Contract No. W31-109-Eng-38 is also gratefully acknowledged. Mr Mark Hash (ANL) is thanked for technical assistance. We would also like to thank Professor Steve Hackney and Ms Yang Shao-Horn, from the Department of Metallurgical and Materials Engineering, Michigan Technological University, for the XRF measurements.

References

[1] M.M. Thackeray, M.H. Rossouw, A. de Kock, A.P de la Harpe, R.J. Gummow, K. Pearce and D.C. Liles, *J. Power Sources, 43–44* (1993) 289–300.
[2] R.J. Gummow, A. de Kock and M.M. Thackeray, *Solid State Ionics, 69* (1994) 59.
[3] M M. Thackeray, W.I.F. David and J B Goodenough, *Mater. Res. Bull., 17* (1982) 785.
[4] M.A Humbert, Ph. Biensan, M. Broussely, A Lecerf, A. Dollé and H Ladhilly, *J. Power Sources, 43–44* (1993) 681.
[5] A. Lecerf, F. Lubin and M. Broussely, *US Patent No. 4 975 346* (1990)
[6] J. Brenet, *J. Power Sources, 39* (1992) 349.
[7] M.H. Rossouw, D.C. Liles and M.M. Thackeray, *Prog. Batteries Battery Mater., 15* (1996) 8.
[8] M.H. Rossouw, D.C. Liles, M.M. Thackeray, W.I.F David and S. Hull, *Mater. Res. Bull., 27* (1992) 221.
[9] P. Rousseau, in D. Glover, B. Schumm Jr and A. Kozawa (eds.), *Handbook on Manganese Oxides Battery Grade*, The International Battery Association Inc., Brunswick, OH, USA, 1989, p. 25.
[10] A.C. Larson and R.B. Von Dreele, GSAS-General Structure Analysis System, *Rep No. LA-UR-86-748*, Los Alamos National Laboratory, Los Alamos, NM 87548, USA, 1990.
[11] JCPDS Powder Diffraction File, *No. 44-0141*, 1992.

[12] A.F. Wells, *Structural Inorganic Chemistry*, Clarendon Press, Oxford, 4th edn., 1975, p. 458.
[13] D.J. Jones, J. Penfold, J. Tomkinson and J. Rozière, *J. Mol. Struct.*, *197* (1989) 113.
[14] F. Fillaux, H. Ouboumour, C. Cachet, J. Tomkinson, G.J. Dearley and L.T. Yu, *Chem. Phys.*, *164* (1992) 311.
[15] J.M. Tarascon and D. Guyomard, *J. Electrochem. Soc.*, *138* (1991) 2864.
[16] Ph. Botkovitz, R. Brec, Ph. Deniard, M. Tournoux and G. Burr, *Mol. Cryst. Liq. Cryst.*, *244* (1994) 233.
[17] Ph. Botkovitz, Ph. Deniard, M. Tournoux and R. Brec, *J. Power Sources*, *43–44* (1993) 657.
[18] M.F. Mansuetto, D.W. Dees, C.S. Johnson, M.M. Thackeray, D.R. Vissers and L. Christensen, *XVII Congr. General Assembly of the International Union of Crystallography, 8–17 Aug. 1996, Seattle, WA, USA*, Abstract accepted for publication.